A Statistical Analysis of Cavitation Erosion Pits

B. Belahadji, Jean-Pierre Franc, Jean-Marie Michel

A Statistical Analysis of Cavitation Erosion Pits

B. Belahadji

J. P. Franc

J. M. Michel

Institut de Mécanique de Grenoble,
Grenoble, France

An optical interferometric technique has been used to determine the 3-D shape of cavitation erosion pits. The method which is particularly suitable to the determination of pit diameter and pit depth is used for a statistical analysis of cavitation erosion pits. We analyzed numerous samples which were eroded at various velocities with two different fluids (mercury and water) on two geometrically similar venturi test sections of different length scales. General properties of histograms of pit size are pointed out. The influence of flow velocity on pitting rates corresponding to limited ranges of pit size is discussed. The contribution of each pit diameter to the total eroded surface is analyzed. Some results are given on pit depths and pit volumes.

1 Introduction

In cavitation erosion studies, several techniques may be used to quantify the damage on a material as pit counting (Stinebring, 1976), measurement of mean depth of deformation (Kato, 1975), or weight loss. Concerning the pit counting technique to which the present paper is devoted, the more studied parameter is pitting rate, i.e., the density of pits per unit surface area and per unit time of exposure, notwithstanding any pit size parameter. In the present analysis, we try to improve this technique in taking into account pit diameter and if possible pit depth. Then, damage is basically characterized by a histogram in size of pit density.

Such an approach describes more precisely the damage on a material as the contribution of small pits or large ones is obviously not equivalent. Even if only total pit density is of interest, discussion of results may be significantly complicated by the cut-off size which is characteristic of the counting technique used.[1] Pitting rate is actually strongly dependent upon this threshold size. In addition, pit size appears as an essential parameter in many studies. It is the case in cavitation erosion scaling which is the main motivation of the present research. In particular, for geometrically similar cavitating flows, an important point is to know how pit size is correlated to the general length scale and how the cut-off size has to be scaled to make relevant comparisons of total pitting rates. Taking into account pit size leads necessarily to a more complicated treatment. For the present research, a specific technique based upon an interference method has been developed. Its principle is described in section 2. It proved to be handy enough and quite suitable to the determination of histograms in size.

The present study is part of a program on cavitation erosion scaling which is in progress in France. Previous experiments (Lecoffre et al., 1985) allowed us to ascertain some scaling assumptions but a few points remained uncleared and required the determination of histograms in size. A large number of samples were eroded in this study under various conditions of flow velocity, fluid and geometric scale as presented in section 3. It is a storehouse of information that we tried to exploit. This paper is devoted to the presentation of the most reliable results we have obtained at the present time. A few points related to scaling rules are still under examination and require additional erosion tests.

2 Pit Analysis Technique

The pit analysis technique used in the present study was developed by G. Tribillon at the "Laboratoire d'Optique de Besançon" in France (Pierali and Tribillon, 1987; Pierali, 1989). It is based upon an interference method schematically presented in Fig. 1. A typical interferogram is given in Fig. 2.

The system is made of a metallographic microscope used with interferential objectives of Mirau type. The light source is a 100W mercury lamp equipped with a green filter centered on wavelength $\lambda = 0.546\mu m$. The light is divided into two

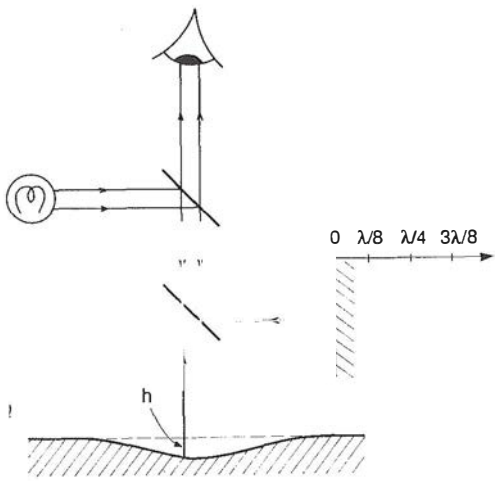

Fig. 1 Principle of the interference method

[1] And possibly of the degree of polish of the surface.

Fig. 2 Typical Interferogram (photograph)

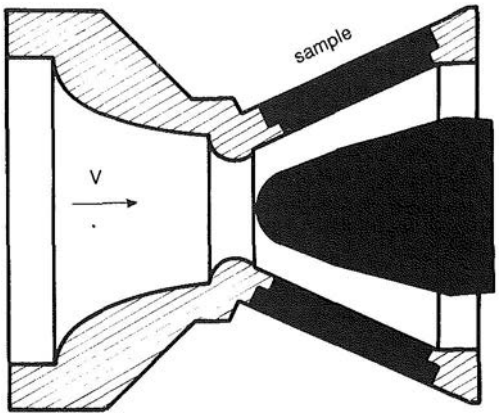

Fig. 3 Geometry of test sections

beams: a reference beam reflected by the mirror of the interferential objective and a second beam reflected by the deformed surface of the eroded sample.

At each point (x,y) of the observed surface, the light intensity I which results from the interference is given by:

$$I(x,y) = I_0 \left(1 + \gamma \cos 2\pi \frac{\delta(x,y)}{\lambda}\right) \tag{1}$$

where I_0 is the incident intensity, γ the fringe contrast, and δ the length difference between the two beams which depends upon pit depth h at location (x,y). In order to determine δ and consequently h and to get rid of constants I_0 and γ, the method developed by Tribillon consists in considering four different interferograms. They are obtained by successive translations of $\lambda/8$ of the reference mirror as shown on Fig. 1.

The four corresponding beam length differences and intensities are given by:

$$\delta_1 = -2h \qquad I_1 = I_0 \left(1 + \gamma \cos \frac{4\pi h}{\lambda}\right)$$

$$\delta_2 = \frac{\lambda}{4} - 2h \qquad I_2 = I_0 \left(1 + \gamma \sin \frac{4\pi h}{\lambda}\right)$$

$$\delta_3 = \frac{\lambda}{2} - 2h \qquad I_3 = I_0 \left(1 - \gamma \cos \frac{4\pi h}{\lambda}\right)$$

$$\delta_4 = \frac{3\lambda}{4} - 2h \qquad I_4 = I_0 \left(1 - \gamma \sin \frac{4\pi h}{\lambda}\right),$$

and from these formula, it can easily be shown that:

$$\frac{h}{\lambda/2} = \frac{1}{2\pi} \operatorname{Arctg} \frac{I_2 - I_4}{I_1 - I_3} \tag{2}$$

This expression proves that, at any point (x,y), the local depth h can be deduced from the four interferograms. Then it is possible to reconstruct the whole surface $h(x,y)$ of the sample under observation. In practice, the four interferograms are obtained by the displacement of the interferential objective by means of a piezoelectric transducer. The acquisition is made by a CCD camera and images of size 512×512 are stored and processed on a microcomputer. Three different magnifications have been used: $\times 10$, $\times 20$ and $\times 40$. With magnification $\times 40$, the size of the observed field is 0.142mm $\times$ 0.201mm.

From Eq. (1), it can be seen that the difference of altitude between two consecutive black fringes is $\lambda/2$. If grey levels are digitized on 8 bits, depth accuracy is of the order of only $\lambda/512$. Thus, the method is very sensitive to small differences in depth.

This high accuracy in depth is at the origin of a difficulty. If the local slope of a pit is too large, the CCD camera may not be able to distinguish two consecutive fringes. This leads to a loss of determination of function Arctg in Eq. (2) and then to the indefiniteness of pit depth. The limitation depends on magnification which determines space resolution. For magnification $\times 40$, the limit slope is approximately 34 deg whereas it is only 10 deg for magnification $\times 10$.

This problem can be limited by increasing computational tests to try to follow the determination of function Arctg. In a few cases, this difficulty is only partially overcome and computed surfaces present depth discontinuities. It is often the case for pits obtained with mercury as their depth is generally an order of magnitude greater than for water (see section 7).

As pits are generally circular, it is enough to restrict shape computation to a unique section going through its center. This procedure allows to reduce considerably computational times, what is essential when the method is implemented on a microcomputer. In the present work, pit diameter D is determined from a unique cross-section chosen visually. It is defined at 10 percent of pit depth.[2] The total surface which is analyzed is such that the number of pits lies between 150 and 200. Such a number proved to be enough to make relevant statistics and not too large to allow a rapid enough analysis. Several images close together are successively treated. Their number vary between 20 and 250 according to degree of erosion.

3 Characteristics of Eroded Samples

The samples which are analyzed in the present study were eroded on geometrically similar flows (Lecoffre et al., 1985). The basic geometry is a venturi shown in Fig. 3 with a central body. Cavitation appears in the form of a small cavity attached to the throat. It sheds vapour structures which collapse downstream and cause cavitation erosion. Samples are flush mounted on the diverging part. The table below presents the main test conditions.

[2]This choice is not purely conventional, as explained in section 4.

Nomenclature

D = pit diameter
h = pit depth
I = light intensity
V = flow velocity
δ = length difference between the two beams
λ = light wavelength
σ = cavitation parameter

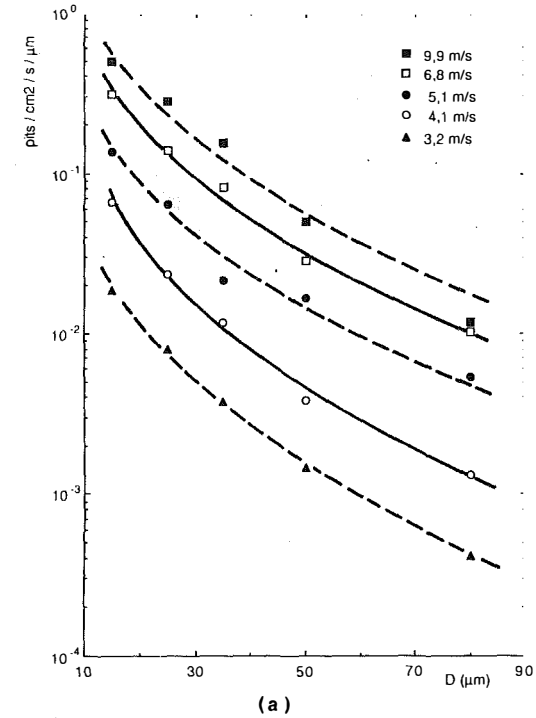

(a)

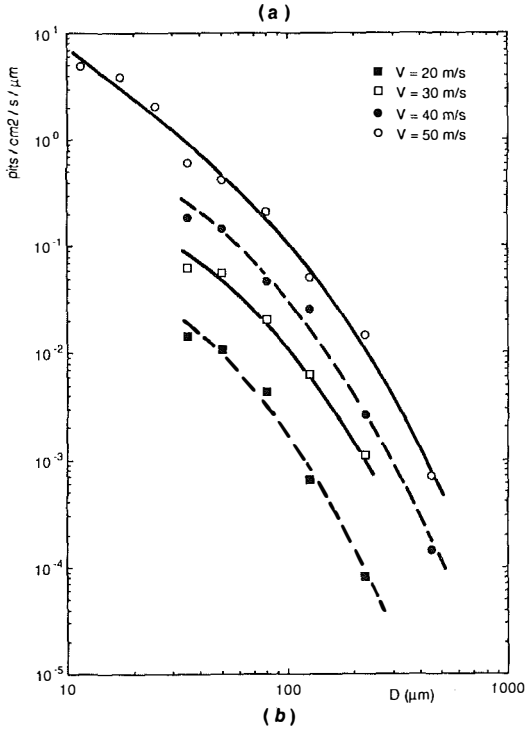

(b)

series N°	throat diameter (mm)	liquid	velocity (m/s)
1	Φ 40	mercury	1.9 to 9.9
2	Φ 40	water	20 to 57
3	Φ 120	water	20 to 57

Cavitation parameter (σ) defined by the ratio of downstream to upstream pressure was kept constant, which ensures a similar development of cavitation.

The tested material is stainless steel 316L. A few tests were carried out with aluminum for cavitation in water. In spite of a very short exposure to cavitation of the order of one minute, the surface was so much eroded that the present method, particularly suitable to isolated pits, could not be applied.

4 Histograms of Pit Diameter

Typical histograms of pit diameter are shown in Fig. 4. The

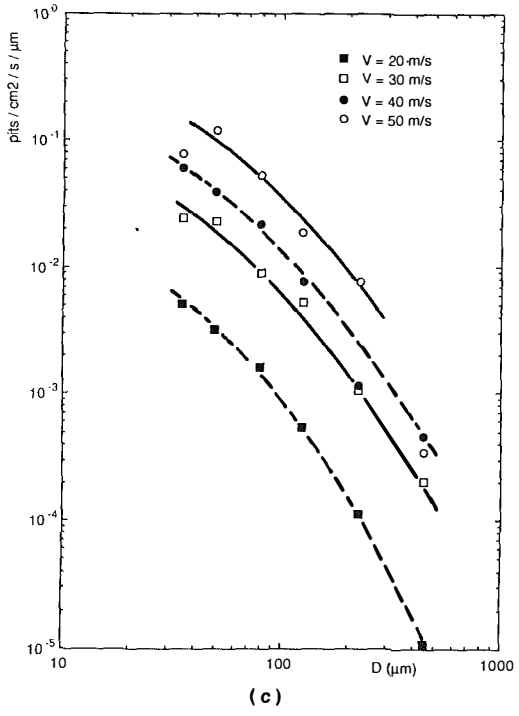

(c)

Fig. 4 (*a*) **Histogram of pit diameter—series No. 1**
(*b*) **Histogram of pit diameter—series No. 2**
(*c*) **Histogram of pit diameter—series No. 3**

ordinate is measured in pits/cm^2/s/μm; the μm dependency appears after dividing pitting rate in pits/cm^2/s by pit size bandwidth. Another type of representation named cumulative histogram is also used (Fig. 5 for instance); in that case the ordinate is measured in pits/cm^2/s and represents the density of pits of diameter greater than a given size plotted in abscissa.

Figure 4 shows, in all cases, that the smaller pits, the higher pitting rates. Contrary to Kato (1989), our histograms do not have a maximum for a given pit size.

For each series, histograms at different velocities have similar shapes. They can easily be superposed if a constant multiplying coefficient is applied to pitting rates. This is shown in Fig. 5 which presents reduced histograms. The coefficient depends only upon velocities and can be considered as independent of pit diameter.

In Fig. 5(*a*) we also plotted the total pitting rate corresponding to the limit $D = 0$ for the mercury tests. Total pit densities were obtained previously with a different counting technique (Lecoffre et al., 1985). The coefficients which were used to get the superposition of histograms in the range of diameter 10μm–90μm appear still valid for total pitting rates though they were determined by a quite different method. The present method allows to measure pits down to 10μm in diameter. The upper limit is given by the size of the image; it is of the order of a few hundreds of μm.

It is possible to measure pits smaller than 10μm; but, the smaller pits, the greater number we may overlook. This tends to make pitting rates decrease artificially for small diameters. In setting the cut-off size at 10μm, we are sure to have, for all diameters, a good determination of pit density.

To determine histograms in the whole range of diameter 10μm–500μm, it is necessary to use two different magnification rates. Magnification $\times 40$ allows to measure pits of diameter between 10μm and 100μm whereas magnification $\times 10$ is suitable to pits between 40μm and 500μm. Figure 6 shows the good comparison between histograms measured with different magnification rates. It was absolutely necessary to check this point in the case of mercury.

In contrast to the water case, the problem of slope limit often arises in mercury, preventing an exact determination of

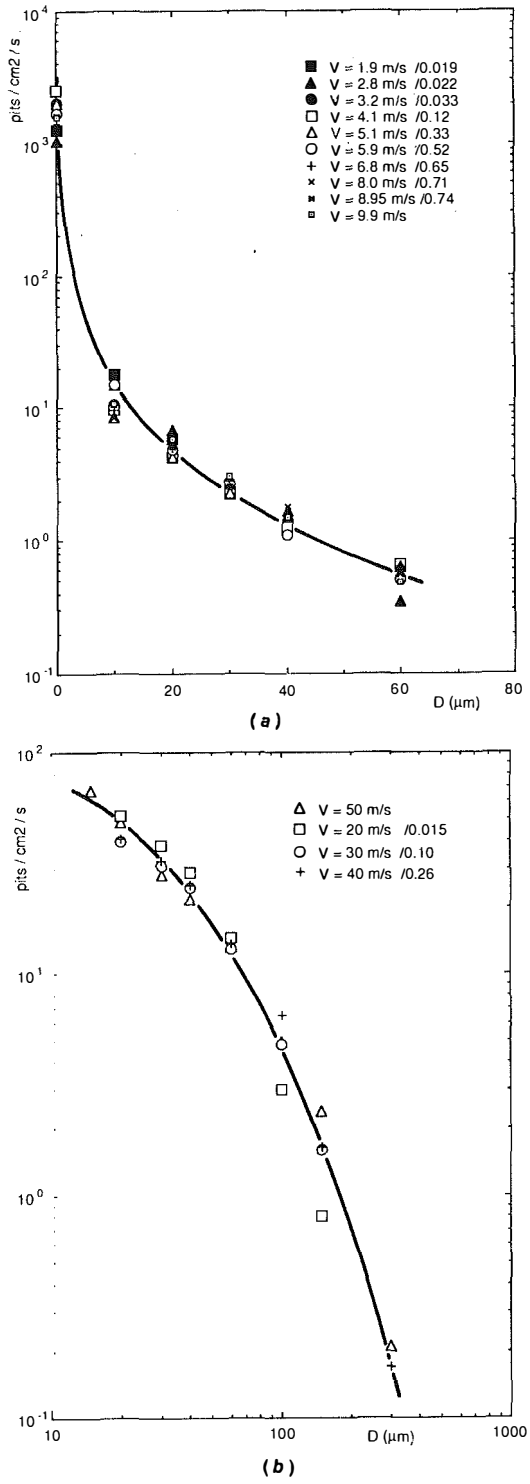

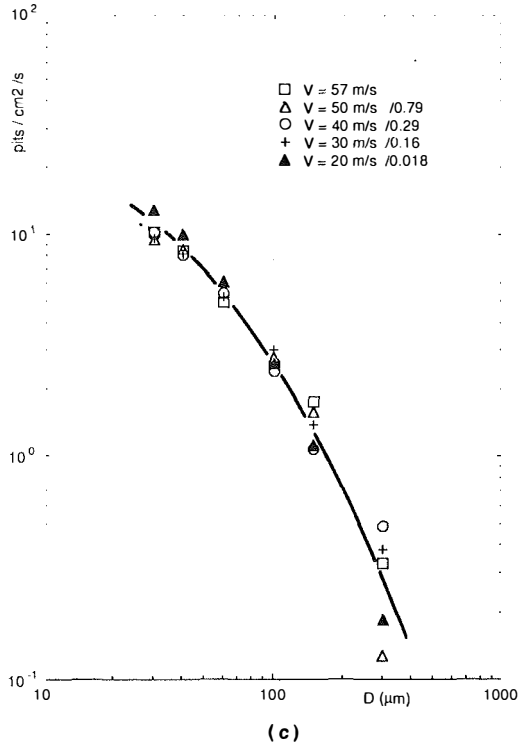

Fig. 5 (*a*) Cumulative reduced histograms—series No. 1 (*b*) Cumulative reduced histograms—series No. 2 (*c*) Cumulative reduced histograms—series No. 3

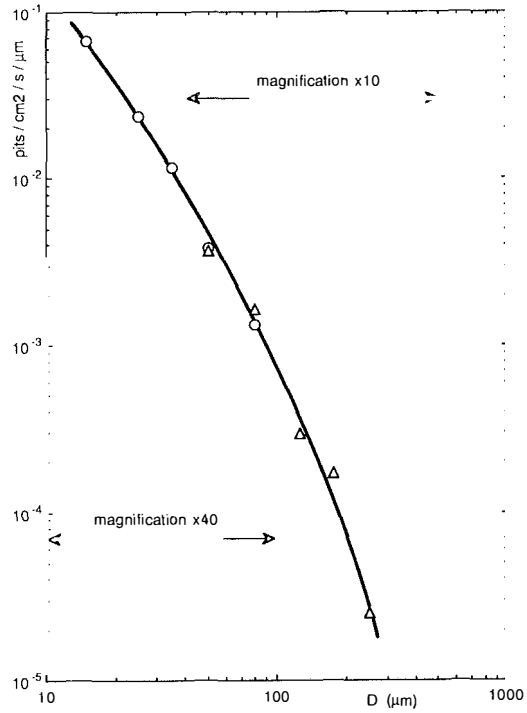

Fig. 6 Histograms measured with different magnifications—series No. 1—*V* = 4.1 m/s

pit depth. The calculated pit profile is regular and can be considered as exact in its outer part where the shape is weak, but becomes discontinuous and so unreliable in its inner part. The frontier between the two domains depends upon the slope limit which increases with magnification (see section 2). The estimated value of pit depth is generally wrong and paradoxically tends to increase with magnification.[3] This difficulty could alter the determination of pit size as pit diameter is defined at a given fraction (k) of pit depth.[4] In fact, the correct junction between histograms in Fig. 6 proves that, even if pit depth remains undetermined in mercury, estimations of pit diameter can be considered as reliable.

To obtain a good estimate of pit size, on the one hand, the value of k has to be low enough to be sure that pit diameter is calculated in the outer region where pit shape is correctly determined. On the other hand, it has to be large enough so that pit diameter is determined in a region of sufficiently high

[3]Even with the greatest magnification ×40 available, pit depth is underestimated in most cases for mercury.

[4]Here $k = 10$ percent.

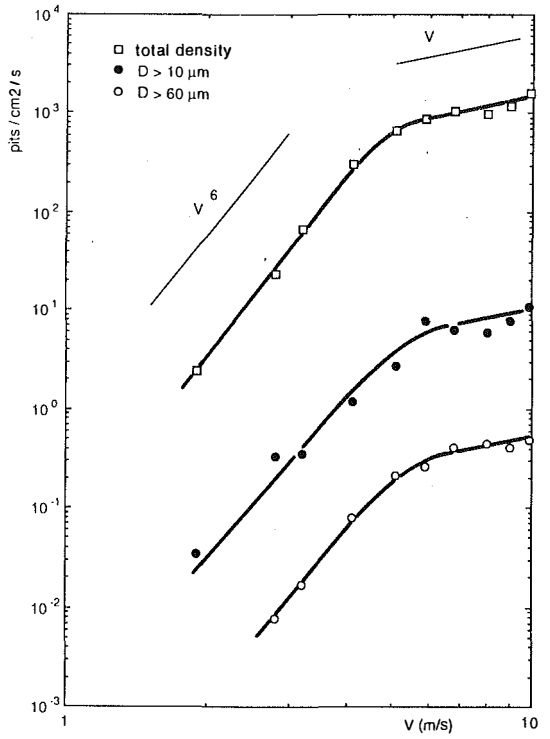

Fig. 7 Influence of velocity on pitting rates for different cut-off diameters—series No. 1

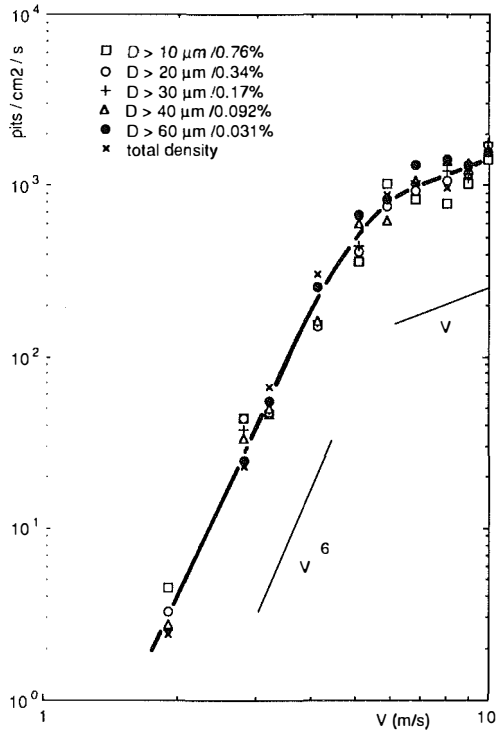

Fig. 8 Reduced pitting rates for different cut-off diameter—influence of velocity—series No. 1

slope where an error in depth generates a low enough error in diameter. In practice, the value $k = 10$ percent gives a good compromise.

5 Influence of Flow Velocity

In the present section, we examine the dependence of pitting rate with flow velocity. It is generally assumed that pitting rate increases as a high power V^n of the velocity which is of the order of 6 (see for instance Stinebring et al., 1980). This trend is valid in a limited range of velocity and the exponent (n) should tend to 1 at high enough velocity. It is the phenomenon of "saturation" presented below and discussed in more details by Lecoffre et al. (1985).

We do not want to discuss here in details the value of n. Our purpose is rather to know if the cut-off size has an influence on the velocity dependence and if partial pitting rates corresponding to limited ranges of pit have different behaviors with velocity or not.

Figure 7 presents the influence of velocity on pitting rates estimated for different cut-off sizes in the case of mercury erosion tests. It appears that the three curves have similar shapes and can be superposed by applying a constant multiplying coefficient independent of velocity (see Fig. 8). The same conclusion also applies to the two other series in water at two different length scales.[5] We now can conclude that a change in velocity affects equally all sizes. Density of small pits or large ones increases with velocity according to the same law.

The phenomenon of saturation in mercury at high enough velocity which was discussed elsewhere (Lecoffre et al., 1985) and which was initially established for total pitting rate appears valid independently for any size. If we consider only pits of a given size, their density increases proportionally to the flow velocity above a threshold of about 5m/s and this behavior applies to any size. Note that saturation was not seen for the data in water up to 57 m/s which is in agreement with the similarity laws developed by Lecoffre et al. (1985).

If we define $n_V(D)$ as the density of pits whose diameter is greater than D at velocity V, we can express mathematically the preceding results by the complete separation of variables D and V. In addition, if the influence on pitting rate of the velocity is known for a given reference size D_o, the histogram $n_V(D)$ at any velocity V can easily be deduced from a reference histogram $n_{V_0}(D)$ obtained for a given reference velocity V_o from the following equation:

$$n_V(D) = \frac{n_V(D_0)}{n_{V_0}(D_0)}\, n_{V_0}(D) \tag{3}$$

This point introduces a significant simplification for the determination of a family of histograms $n_V(D)$ corresponding to different velocities. This result is applied in this paper for cumulative histograms but also applies to spectra.

6 Eroded Surface

Histograms in size show a very rapid increase of pitting rate when pit size decreases. However, we can expect that small impacts cause smaller damage than larger ones, at least if damage is measured from eroded surfaces as it is the case in the present section. Then, the question is to compare the contributions of all sizes to total erosion and in particular to know if small pits which are very numerous contribute significantly or not to cavitation erosion.

Figure 9 presents, for the case of mercury, the eroded surface per class of diameter. All curves corresponding to different velocities show a maximum for a given pit size of the order of 30μm. This characteristic size is independent of flow velocity, which comes out of the existence of reduced histograms. The existence of this maximum means, on the one hand, that large pits are not numerous enough to erode the surface significantly, whereas, on the other hand, small pits concern a negligible surface although their density is very high.

In the case of water, similar results were obtained. For a throat diameter of 40mm (series 2), the characteristic diameter

[5]Corresponding diagrams are not presented here.

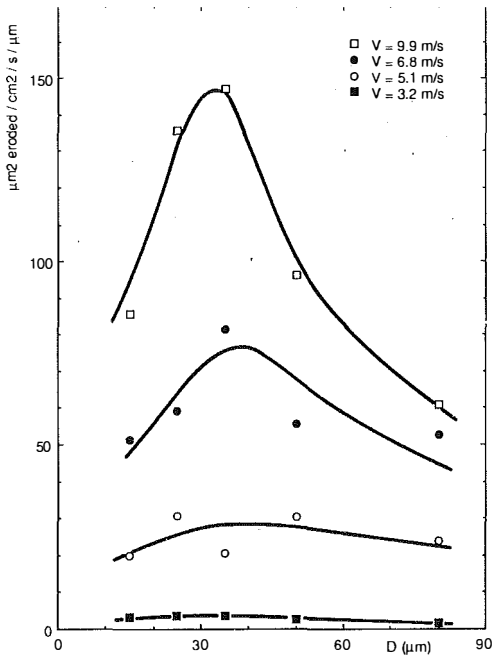

Fig. 9 Eroded surface per class of diameter—series No. 1

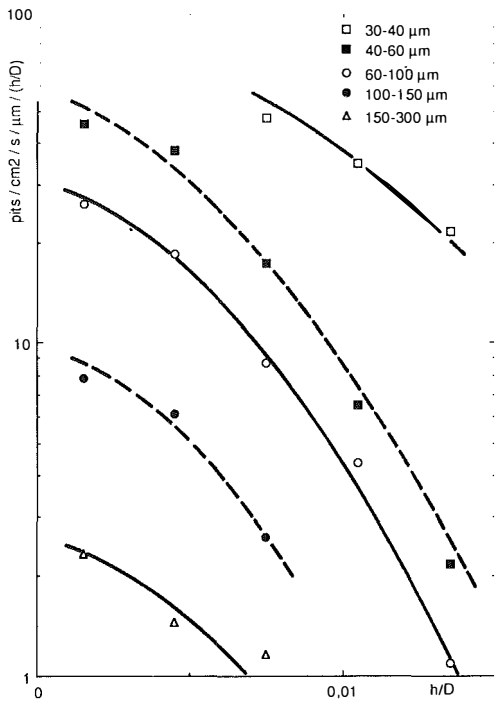

Fig. 10 Histograms of relative pit depth for various classes in diameter—series No. 2—V = 57 m/s

for which the eroded surface is maximum is of the order of 70μm. For a throat diameter of 120mm, this characteristic size is increased, but less than the global length scale; it is of the order of 100μm.

The estimation of the total eroded surface obtained in taking into account all sizes allows to determine the fraction of surface eroded per unit time of exposure. It gives a global estimate of the probability of overlapping of impacts according to the time of exposure. For example, from erosion tests of series 2 in water, and in considering all pits in the range 30μm-600μm, the ratio of the eroded surface to the exposed surface is 7.2 percent at 20m/s and 650 percent at 57m/s, per hour of exposure.

7 Pit Depth and Pit Volume

Pits are generally not very deep. Their reduced depth h/D is, in the case of water, generally smaller than 1 percent. It means that a pit of 0.1mm in diameter is less than 1μm deep. We could not determine pit depth owing to the problem of slope which was previously discussed for the case of mercury. However, we can roughly estimate that pits due to cavitation in mercury are deeper than for water. A value of reduced depth of a few percents seems most likely.

As a first approach, we calculated the mean values and rms values of reduced depth h/D for water. We did not notice any regular variation of reduced depth with pit diameter. On an average, large pits are not proportionally deeper than small ones; we can consider that mean shapes are similar. Yet, if we consider all pits of a given diameter, a great scattering in depth is observed. It shows that, even if pits can be statistically characterized by a mean shape independent of their size, there is a large variety of shapes around it.

The only systematic variation which could be pointed out is relative to flow velocity. In considering all pits of size between 30μm and 600μm, we obtained the following results:

	$V(m/s)$	20	30	40	50	57
h/D	series 2	0.26	0.35	0.33	0.42	0.51
(%)	series 3	0.32	0.38	0.37	0.43	0.50

The general trend is an increase of relative pit depth with velocity. Between 20m/s and 57m/s, h/D is multiplied by a coefficient of about 1.5 or 2.

As a second approach, we tried to introduce two-dimensional histograms, one dimension being pit size and the other dimension being pit depth. A typical two-dimensional histogram is given in Fig. 10. For all sizes, histograms of relative pit depth show the same trend. There is a continuously increasing number of pits which correspond to weaker and weaker deformations of the surface. This implies that there is no mean depth for pits of a given size. Mean values which were presented above are simply relative to a statistics on all pits which were taken into account i.e., which depth is greater than approximately $\lambda/4 \cong 0.1\mu$m.

The problem of the cut-off depth appears to be very similar to the one of the cut-off size discussed previously. Undoubtedly, two-dimensional histograms give a better description of cavitation damage, but the introduction of a second dimension brings new difficulties. In the case of water for which pit depth could be measured, it was also possible to determine pit volumes. They were calculated by rotating the pit profile and calculating the generated volume.

In the same way as we discussed the contribution of all sizes to the total eroded surface, we can easily estimate the contribution of all sizes to the "eroded volume." By eroded volume, we mean the cumulative volume of pits. As pits are only permanent deformations without material removal, such a data is not representative of mass loss.

Figure 11 presents, in the cases of erosion tests of series 2 in water, the distribution of eroded volumes with pit size. Results are quite similar to the ones obtained for eroded surfaces. In particular, there is a characteristic size for which the eroded volume shows a maximum. Larger pits give a smaller contribution due to their small density whereas smaller ones, although they are very numerous, have also a contribution of minor importance. The characteristic size for which the eroded volume is maximum is slightly greater than the one for which the eroded surface is maximum. For series 2 and 3, it is, respectively, of about 100μm and 200μm.

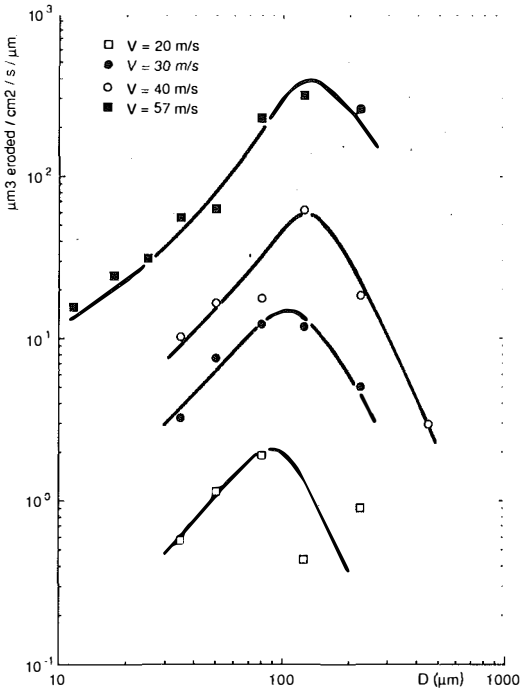

Fig. 11 Eroded volume per class of diameter—series No. 2

8 Uncertainty Estimates

For histograms (Figs. 4, 5, 6, 9, 10, 11) the uncertainties on abscissae D or h/D can be considered as negligible. Same conclusion for the abscissae of Figs. 7 and 8 which correspond to the velocity in the testing facility and which is known with a very good accuracy.

Uncertainty on pitting rates is estimated to ± 25 percent for $D \leq 200\mu$m. Large pits are less numerous and errors of statistical nature are greater; for $D > 200\mu$m, the uncertainty on pitting rate is estimated to ± 40 percent. Such uncertainties may appear quite large but represent in fact only a small fraction of full scale as pitting rate extends over several decades.

9 Conclusion

This paper presents an analysis of histograms in size of erosion pits. An interferometric method originally developed by Pierali and Tribillon (1987) was adapted to cavitation erosion in order to measure pit size. It is particularly suitable for pits of diameter in the range 10μm-500μm. Conclusions of this paper were focused on general properties of histograms. They were established for three conditions of erosion with two different fluids (mercury and water) on two similar test sections of different length scale. The following summarizes the important conclusions:

1. Histograms in size corresponding to different flow velocities can be reduced to a unique histogram by means of a multiplicative factor on pitting rates which is independent of diameter and depends only of flow velocity. Histograms have similar shapes whatever the flow velocity may be, i.e., pits are distributed among the different sizes in a similar way independent of flow velocity.

2. The influence of velocity on pitting rate is the same whatever the considered size may be. In particular, its influence is the same as for total pitting rate. In the case of erosion with mercury, it is shown that saturation, which was initially pointed out at high enough velocity for total pitting rate, applies individually to partial densities of pits of any given size.

3. Concerning eroded surface, all analyses have pointed out a characteristic size for which the contribution to the eroded surface is maximum. Smaller pits, although they are more numerous, have a minor contribution whereas larger ones have also a minor contribution but because of their small number. For stainless steel, this characteristic size is of the order of:

30μm for erosion in mercury on a venturi of 40mm in throat diameter

70μm for erosion in water on the same venturi of 40mm in throat diameter

100μm for erosion in water on the same venturi of 120mm in throat diameter.

4. Reduced pit depth h/D tends to increase with flow velocity. No correlation of pit depth with diameter was observed. On an average, pits have similar shapes, although there is a large scattering in shapes.

5. Eroded volumes as eroded surfaces present a maximum for a given pit size slightly greater than the one for eroded surfaces.

Further work, requiring complementary tests, is in progress to interpret such histograms in terms of scaling laws for cavitation erosion.

Acknowledgment

This research was supported by "Electricité de France" and C.E.R.G.

References

Kato, H., 1975, "A Consideration on Scaling Laws of Cavitation Erosion," *International Shipbuilding Progress*, Vol. 22, No. 253, pp. 305-327.

Kato, H., Ye, Y. P., and Maeda, M., 1989, "Cavitation Erosion and Noise Study on a Foil Section," *ASME Intern. Symp. on Cavitation Noise and Erosion in Fluid Systems*, San Francisco.

Lecoffre, Y., Marcoz, J., Franc, J. P., and Michel, J. M., 1985, "Tentative Procedure for Scaling Cavitation Damage," *ASME Intern. Symp. on Cavitation in Hydraulic Structure and Turbomachinery*, Albuquerque.

Pierali, C., 1989, "Traitement numérique d'interférogrammes et applications à la caractérisation tridimensionnelle des phénomènes d'érosion de cavitation," Thèse Université de Franche-Comté, Besançon.

Pierali, C., and Tribillon, G., 1987, "Traitement d'images 3D appliqué à la profilométrie optique pour l'étude du phénomène d'érosion de cavitation," *J. Optics* (Paris), Vol. 18, No. 1, pp. 9-18.

Stinebring, D. R., 1976, "Scaling of Cavitation Damage," MS thesis, The Pennsylvania State University.

Stinebring, D. R., Holl, J. W., and Arndt, R. E. A., 1980, "Two Aspects of Cavitation Damage in the Incubation Zone: Scaling by Energy Considerations and Leading Edge Damage," ASME Journal of Fluids Engineering, Vol. 102, pp. 481-485.